Journal of Thermal Analysis and Calorimetry (2021) 143:915–927
https://doi.org/10.1007/s10973-020-09602-1

Magnetohydrodynamic flow of $Cu–Fe_3O_4/H_2O$ hybrid nanofluid with effect of viscous dissipation: dual similarity solutions

Liaquat Ali Lund[1,2] · Zurni Omar[1] · Jawad Raza[3] · Ilyas Khan[4]

Received: 2 December 2019 / Accepted: 18 March 2020 / Published online: 9 April 2020

Abstract
This study shows multiple solutions, heat transfer characteristics, and stability analysis of the magnetohydrodynamic (MHD) flow of hybrid nanofluid caused by the nonlinear shrinking/stretching surface. To investigate the effects of high temperature on the porous surface, the energy dissipation function and porous term are considered in the momentum and energy equations. We used Tiwari and Das's model for nanofluid in which water is considered as a base fluid. A new kind of fluid is made in which two kinds of nanoparticles, namely copper (Cu) and iron oxide (Fe_3O_4), are considered. The system of ordinary differential equations (ODEs) is obtained by applying similarity transformations on the modeled of partial differential equations. Both shooting and Runge–Kutta fourth-order methods are employed to solve the resultant ODEs. The equations for stability analysis have been derived and then solved by using a three-stage Lobatto IIIa formula for the smallest eigenvalue. It is noticed that the obtained value is in a good agreement with the previously published literature, hence validating the results of the shooting method. Furthermore, parametric studies also have been conducted and found that dual solutions only exist on the shrinking surface. In addition, it is also observed from the profile that dual solutions exist only for the case of suction where $b_{c1} = -3.0582$, $b_{c2} = -3.0788$, and $b_{c3} = -3.1249$ are the critical values for the respective values of $\phi_{Fe_3O_4} = 0.5\%, 5\%, 1\%$. Moreover, the velocity of hybrid nanofluid decreases (increases) in the first (second) solution when both magnetic and permeability coefficient parameters are increased.

Keywords $Cu - Fe_3O_4/H_2O$ · Hybrid nanofluid · Dual solutions · Stability analysis · MHD

List of symbols

T_0	A constant
T_∞	Ambient temperature
$'$	Differentiation with respect to
Ec	Eckert number
ρ_{hnf}	Effective density of hybrid nanofluid
ρ_{nf}	Effective density of nanofluid
μ_{hnf}	Effective dynamic viscosity of hybrid nanofluid
μ_{nf}	Effective dynamic viscosity of nanofluid
σ^*	Electrical conductivity
f	Fluid fraction
M	Hartmann/magnetic number
$(\rho c_p)_{hnf}$	Heat capacitance of the hybrid nanofluid
$(\rho c_p)_{nf}$	Heat capacitance of the nanofluid
hnf	Hybrid nanofluid
N_u	Local Nusselt number
Re	Local Reynolds number
B	Magnetic field
nf	Nanofluid fraction
ϕ_{Cu}	Nanoparticle volume fraction of the copper
$\phi_{Fe_3O_4}$	Nanoparticle volume fraction of the iron oxide
K	Permeability parameter
K_1	Porous parameter
m	Positive constant
Pr	Prandtl number

✉ Ilyas Khan
ilyaskhan@tdtu.edu.vn

Liaquat Ali Lund
balochliaqatali@gmail.com

Zurni Omar
zurni@uum.edu.my

Jawad Raza
jawad_6890@yahoo.com

1 School of Quantitative Sciences, Universiti Utara Malaysia, 06010 Sintok, Kedah, Malaysia

2 KCAET Khairpur Mirs, Sindh Agriculture University, Tandojam 70060, Sindh, Pakistan

3 Department of Mathematics and Statistics, Institute of Southern Punjab (ISP), Multan, Pakistan

4 Faculty of Mathematics and Statistics, Ton Duc Thang University, Ho Chi Minh City, Vietnam

C_f	Skin friction coefficient
γ_1	Smallest eigenvalue
τ	Stability transformed variable
v_w	Suction/injection velocity
T	Temperature
k_{hnf}	Thermal conductivity of the hybrid nanofluid
k_{nf}	Thermal conductivity of the nanofluid
t	Time
η	Transformed variable
γ	Unknown eigenvalue
T_w	Variable temperature at the sheet
u, v	Velocity components
u_w	Velocity of shrinking/stretching surface
b	Suction parameter and blowing parameter

Introduction

In the present decade, researchers are interested in mixing up different nanoparticles with different base fluids in order to enhance the thermal conductivity of regular fluids such as water, propylene glycol, ethylene glycol, and kerosene oil. The resultant fluids, known as nanofluids, have different characteristics and can be used in biomedical applications in cooling, engineering, process industries, and cancer therapy. Thermal conductivity and heat transfer of convectional fluids are enhanced by dispersing the solid particles in the recent advances in nanotechnology and engineering. It is worth to highlight that the heat transfer coefficient increases as expected after the suspension of these particles. Physically, it is possible because the thermal conductivity of solid particles, such as metal and carbon nanotubes, is higher than that of regular base fluids. Therefore, heat transfer and thermal conductivity are enhanced. There are many advantages of these fluids such as better wetting, sufficient viscosity, and more stability [1]. Some commonly used nanoparticles are oxides (Al_2O_3), metals (Al, Ag, Cu), nitrides (AlN, SiN), nonmetals (graphite, carbon nanotubes), carbides (SiC), etc. Generally, the diameter of these nanoparticles is between 1–100 nm. According to experimental studies by researchers [2–8], 5%, 10%, …, 55% volume fraction of nanoparticles are considered for a better rate of heat transfer and thermal conductivity of base fluids. It is discovered that the maximum effective rate of heat transfer is possible when the volume fraction of nanoparticles is 5%. There are many applications where nanofluids are used effectively such as fuel cell, transportation, biomedicine, and nuclear reactors. [9–11]. The better cooling performance, the higher thermal conductivity and the rate of heat transfer can be achieved by using a magnetic force. As an instance, continuous strips and drawing filaments can control the cooling rate with the help of electrically conducting nanofluids [12, 13]. Ferrofluids can be defined as the electrically conducting nanofluids where base fluids contain nanoparticles such as Hematite, Magnetite, Cobalt Ferrite or other compounds having iron. The thermal conductivity of nanofluids depends upon numerous factors such as size, shape, and volume fraction of the solid particles, the surrounding temperature, and base fluid [14–16].

It can be seen that many researchers considered different fluids and particles in order to enhance thermal conductivity. Lund et al. [17] considered sodium alginate as a base fluid in their studies and found dual solutions. Water-based nanofluid was studied by Bhatta et al. [18] and concluded that "enhancement in the heat transfer coefficient is noted due to the interaction of buoyancy parameter". Hayat et al. [19] examined a nanofluid by considering two base fluids, namely kerosene oil and water with carbon nanotubes as the nanoparticles. Selimefendigil et al. [20] investigated Fe_3O_4/water nanofluid in the channel and found that when the volume fraction of nanoparticles is 12–15%, Nusselt number increases more effectively. TiO_2/water nanofluid was investigated by Kristiawan et al. [21] and stated that this nanofluid enhances the heat transfer rate and decreases the pressure. Dero et al. [22] examined Cu/water nanofluid and found dual solutions. Further, they performed a stability analysis to observe a stable solution. Some other development of nanofluid can be seen in these articles [23–29]. It is observed from the previous studies that the thermal conductivity of copper particles is higher as compared to the alumina and other solid nanoparticles. Further, solid particles of iron oxide are important to consider when the magnetic effect is incorporated. Therefore, both copper and iron oxide particles have been considered in this study in order to enhance the heat transfer rate effectively.

There are two fluid models in the computational fluid dynamics (CFD), namely Buongiorno's model [30] and Tiwari and Das's model [31]. Both models have been used intensively when researchers deal with nanofluid by numerical approaches. Due to the presence of nonlinearity in the governing equations, many researchers attempted to find multiple solutions as they have many applications in various fields of science. Khashi'ie et al. [32] successfully found dual solutions for three-dimensional MHD flow of nanofluid. Moreover, they considered Buongiorno's model and examined the effect of thermophoresis and Brownian motion parameters. Mixed convection flow of water-based nanofluid was investigated by Jamaludin et al. [33]. Further, Tiwari and Das's model [31] has been used to deal with governing equations, and they found dual solutions in the ranges of various parameters and performed stability analysis. Ali et al. [34] examined the MHD flow of micropolar nanofluid and found triple solutions. By performing stability analysis, they claimed that only the first solution is stable. Many important related references of non-uniqueness of solutions of nanofluids can be seen in these articles [35–41].

It can be concluded from the above-mentioned studies that researchers are still interested in searching for new kinds of fluids that are more capable of enhancing thermal conductivity and heat transfer rate. In this regard, researchers introduced new kinds of nanofluids called "hybrid nanofluids" recently. They believed that these fluids offer better thermal conductivity as compared to simple nanofluids. Hybrid nanofluid is the extension of nanofluid in which two different kinds of nanoparticles are suspended in a single base fluid [42]. There are many applications in numerous fields such as generator cooling, nuclear system cooling, drug reduction, biomedical, electronic cooling, the coolant in machining, and refrigeration where these kinds of fluid can be used effectively [43]. Ahmed et al. [44] studied hybrid nanofluid by considering nanoparticles and water as a base fluid and found a single solution. Devi and Devi [45] examined the hydromagnetic flow of $Cu - Al_2O_3$/water hybrid nanofluid over the stretching surface and found a single solution. Their work was then extended by Waini et al. [46] for the multiple solutions. In the same year, the unsteady flow of hybrid nanofluid was examined by Waini et al. [47] and dual solutions were successfully noticed. There are only a few researchers who considered hybrid nanofluids for multiple solutions [48–53].

Motivated by the above works, our prime objective of this study is to find multiple solutions of hybrid nanofluid in the presence of magnetic, porous, and viscous dissipation effect over nonlinear permeable shrinking/stretching surfaces theoretically by employing of Tiwari and Das's model [31] which has not been studied before. Two different kinds of nanoparticles are considered, namely Cu (copper) and Fe_3O_4 (iron oxide) in base fluid (water). It is expected that these findings would help those who are interested in increasing the heat transfer rate through experiments and finding multiple solutions for hybrid nanofluids.

Problem formulation

We have considered the two-dimensional laminar flow of electrically conducting hybrid nanofluid on nonlinearly shrinking/stretching surfaces with the effect of porous and viscous dissipation. Water is assumed as a base fluid, and copper and magnetite are considered as nanoparticles. Further, it is also assumed that the magnetic field effect is constant $B = B_0 x^{(1-m)/2}$ and applied in the perpendicular direction to hybrid nanofluid flow. It is also supposed that base fluid and the nanoparticles are in thermal equilibrium. The surface is stretched and shrunk along a velocity $u_w(x) = ax^m$, where a is a constant and m is a power index. Velocity of wall mass suction is $v_w(x) = -b\sqrt{c\vartheta} x^{(m-1)/2}$ as seen in Fig. 1. The external forces and pressure gradients are ignored. By considering all the above assumptions, the governing equations of momentum and heat boundary layers in the model of Tiwari and Das [31] can be written as:

$$\frac{\partial u}{\partial x} + \frac{\partial v}{\partial y} = 0 \tag{1}$$

$$u\frac{\partial u}{\partial x} + v\frac{\partial u}{\partial y} = \frac{\mu_{hnf}}{\rho_{hnf}}\frac{\partial^2 u}{\partial y^2} - \frac{\mu_{hnf}}{\rho_{hnf}}\frac{u}{K_1} - \frac{\sigma^* B^2 u}{\rho_{hnf}} \tag{2}$$

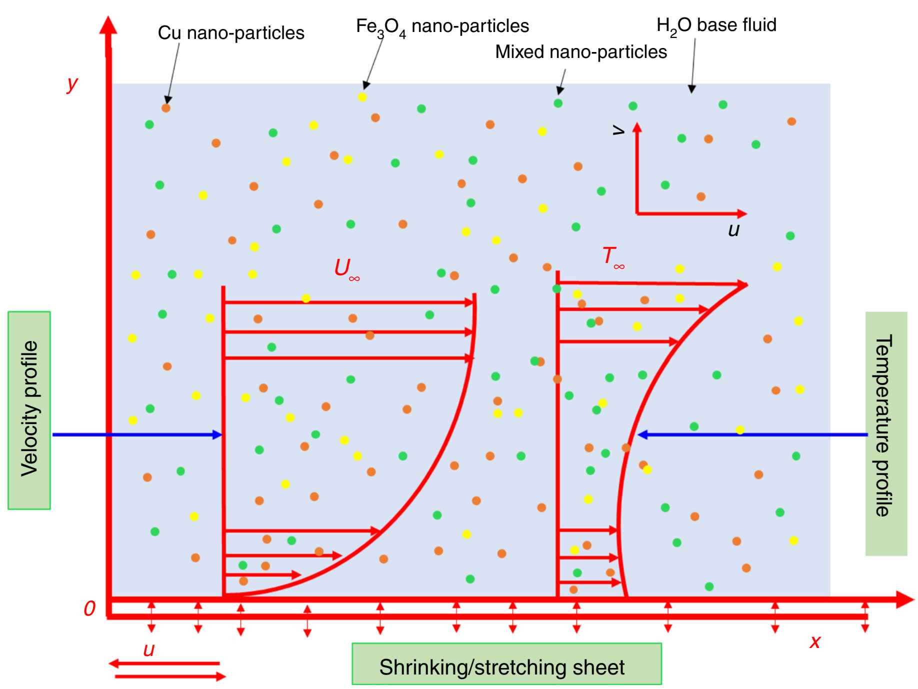

Fig. 1 Physical models and coordinate systems

$$u\frac{\partial T}{\partial x}+v\frac{\partial T}{\partial y}=\frac{k_{\mathrm{hnf}}}{(\rho c_{\mathrm{p}})_{\mathrm{hnf}}}\frac{\partial^2 T}{\partial y^2}+\frac{\mu_{\mathrm{hnf}}}{(\rho c_{\mathrm{p}})_{\mathrm{hnf}}}\left(\frac{\partial u}{\partial y}\right)^2 \tag{3}$$

The subjected boundary conditions are

$$\begin{cases} v=v_{\mathrm{w}}(x), u=u_{\mathrm{w}}(x), T=T_{\mathrm{w}} \text{ as } y\to 0 \\ u\to 0, T\to T_\infty \text{ as } y\to\infty \end{cases} \tag{4}$$

In this study, the following subsequent definitions are used [49–51], which are given in Table 1. Table 2 is constructed for the thermophysical features of nanomaterials and base.

Now, the following variables of similarity transformation are introduced as:

$$\begin{cases} v=-\sqrt{\frac{c\vartheta(m+1)}{2}}x^{(m-1)/2}\left[f(\eta)+\frac{m-1}{m+1}\eta f'(\eta)\right] \\ u=cx^{m}f'(\eta), \eta=y\sqrt{\frac{c(m+1)}{2\vartheta}}x^{(m-1)/2} \\ \theta(\eta)=(T-T_\infty)/(T_{\mathrm{w}}-T_\infty) \end{cases} \tag{5}$$

Table 2 The thermophysical properties of the base fluid (water) and the nanoparticles [13, 63]

Fluids	ρ/kg m^{-3}	c_{p}/J kg^{-1} K^{-1}	k/W m^{-1} K^{-1}
Iron oxide (Fe_3O_4)	5180	670	9.7
Copper (Cu)	8933	385	400
Water (H_2O)	997.1	4179	0.613

The implementation of Eq. (5) into Eqs. (1–3) leads to the subsequent equations

$$f'''+\xi_1\left\{f''f-\frac{2m}{(m+1)}(f')^2\right\}-\frac{2}{(m+1)}\left\{M(1-\phi_{Cu})^{2.5}(1-\phi_{Fe_3O_4})^{2.5}+K\right\}f'=0 \tag{6}$$

$$\frac{\xi_2}{\mathrm{Pr}}\theta''+\theta'f-\frac{4m}{(m+1)}\theta f'+\xi_3\mathrm{Ec}(f'')^2=0 \tag{7}$$

Subject to boundary conditions

$$\begin{cases} f(0)=-b\sqrt{\frac{2}{m+1}}, f'(0)=\lambda, \theta(0)=1 \\ f'(\eta)\to 0, \theta(\eta)\to 0 \text{ as } \eta\to\infty \end{cases} \tag{8}$$

In the above equations, we have

$$\begin{cases} M=\frac{\sigma^* B_0^2}{c\rho_{\mathrm{f}}}, K=\frac{\vartheta_{\mathrm{f}}}{cK_1x^{m-1}}, \lambda=\frac{a}{c}, \mathrm{Pr}=\frac{\vartheta_{\mathrm{f}}}{\alpha_{\mathrm{f}}}, \mathrm{Ec}=\frac{c^2\rho_{\mathrm{f}}}{T_0(\rho c_{\mathrm{p}})_{\mathrm{f}}} \\ \xi_1=(1-\phi_{\mathrm{Cu}})^{2.5}(1-\phi_{\mathrm{Fe_3O_4}})^{2.5}\left\{(1-\phi_{\mathrm{Fe_3O_4}})\left[1-\phi_{\mathrm{Cu}}+\phi_{\mathrm{Cu}}\left(\rho_{\mathrm{Cu}}/\rho_{\mathrm{f}}\right)\right]+\phi_{\mathrm{Fe_3O_4}}\left(\rho_{\mathrm{Fe_3O_4}}/\rho_{\mathrm{f}}\right)\right\} \\ \xi_2=\frac{(k_{\mathrm{hnf}}/k_{\mathrm{f}})}{\left\{(1-\phi_{\mathrm{Fe_3O_4}})\left[1-\phi_{\mathrm{Cu}}+\phi_{\mathrm{Cu}}\frac{(\rho c_{\mathrm{p}})_{\mathrm{Cu}}}{(\rho c_{\mathrm{p}})_{\mathrm{f}}}\right]+\phi_{\mathrm{Fe_3O_4}}\frac{(\rho c_{\mathrm{p}})_{\mathrm{Fe_3O_4}}}{(\rho c_{\mathrm{p}})_{\mathrm{f}}}\right\}} \\ \xi_3=\frac{1}{(1-\phi_{\mathrm{Cu}})^{2.5}(1-\phi_{\mathrm{Fe_3O_4}})^{2.5}\left\{(1-\phi_{\mathrm{Fe_3O_4}})\left[1-\phi_{\mathrm{Cu}}+\phi_{\mathrm{Cu}}\frac{(\rho c_{\mathrm{p}})_{\mathrm{Cu}}}{(\rho c_{\mathrm{p}})_{\mathrm{f}}}\right]+\phi_{\mathrm{Fe_3O_4}}\frac{(\rho c_{\mathrm{p}})_{\mathrm{Fe_3O_4}}}{(\rho c_{\mathrm{p}})_{\mathrm{f}}}\right\}} \end{cases} \tag{9}$$

Table 1 Thermophysical properties of hybrid nanofluid

Properties	Hybrid nanofluid
Dynamic viscosity	$\mu_{\mathrm{hnf}}=\frac{\mu_{\mathrm{f}}}{(1-\phi_{\mathrm{Cu}})^{2.5}(1-\phi_{\mathrm{Fe_3O_4}})^{2.5}}$
Density	$\rho_{\mathrm{hnf}}=(1-\phi_{\mathrm{Fe_3O_4}})\left[(1-\phi_{\mathrm{Cu}})\rho_{\mathrm{f}}+\phi_{\mathrm{Cu}}\rho_{\mathrm{Cu}}\right]+\phi_{\mathrm{Fe_3O_4}}\rho_{\mathrm{Fe_3O_4}}$
Thermal conductivity	$k_{\mathrm{hnf}}=\frac{k_{\mathrm{Fe_3O_4}}+2k_{\mathrm{nf}}-2\phi_{\mathrm{Fe_3O_4}}(k_{\mathrm{nf}}-k_{\mathrm{Fe_3O_4}})}{k_{\mathrm{Fe_3O_4}}+2k_{\mathrm{nf}}+\phi_{\mathrm{Fe_3O_4}}(k_{\mathrm{nf}}-k_{\mathrm{Fe_3O_4}})}\times(k_{\mathrm{nf}})$ where $k_{\mathrm{nf}}=\frac{k_{\mathrm{Cu}}+2k_{\mathrm{f}}-2\phi_{\mathrm{Cu}}(k_{\mathrm{f}}-k_{\mathrm{Cu}})}{k_{\mathrm{Cu}}+2k_{\mathrm{f}}+\phi_{\mathrm{Cu}}(k_{\mathrm{f}}-k_{\mathrm{Cu}})}\times(k_{\mathrm{f}})$
Heat capacity	$(\rho c_{\mathrm{p}})_{\mathrm{hnf}}=(1-\phi_{\mathrm{Fe_3O_4}})\left[(1-\phi_{\mathrm{Cu}})(\rho c_{\mathrm{p}})_{\mathrm{f}}+\phi_{\mathrm{Cu}}(\rho c_{\mathrm{p}})_{\mathrm{Cu}}\right]+\phi_{\mathrm{Fe_3O_4}}(\rho c_{\mathrm{p}})_{\mathrm{Fe_3O_4}}$

The interesting physical quantities are the skin friction coefficient C_f and local Nusselt number Nu_x:

$$C_f = \frac{2\mu_{hnf}}{\rho_f u_w^2}\left(\frac{\partial u}{\partial y}\right)|y=0, Nu_x = -\frac{x k_{hnf}}{k_f\left(T_w - T_\infty\right)}\left(\frac{\partial T}{\partial y}\right)|y=0 \tag{10}$$

By applying Eq. (9) in Eq. (10), we have

$$\begin{aligned}\sqrt{Re}C_f &= \frac{1}{\left(1-\phi_{Cu}\right)^{2.5}\left(1-\phi_{Al_2O_3}\right)^{2.5}}\sqrt{\frac{(m+1)}{2}}f''(0);\\ \sqrt{\frac{1}{Re}}Nu_x &= -\frac{k_{hnf}}{k_f}\sqrt{\frac{(m+1)}{2}}\theta'(0)\end{aligned} \tag{11}$$

where $Re = \frac{cx^m}{\vartheta_f}$ is local Reynolds number.

Stability analysis

There is a problem to know which solution is more stable when more than one solution exists in any fluid model. Researchers created a new method by introducing a new dimensionless time variable τ [47, 48, 54, 55] in which they performed the stability analysis of solutions mathematically. This study is carried out by many researchers in their studies, some of them can be seen in these references [56–59]. The first step of performing the stability of the solution is to change the governing Eqs. (2–3) in unsteady form.

$$\frac{\partial u}{\partial t} + u\frac{\partial u}{\partial x} + v\frac{\partial u}{\partial y} = \frac{\mu_{hnf}}{\rho_{hnf}}\frac{\partial^2 u}{\partial y^2} - \frac{\mu_{hnf}}{\rho_{hnf}}\frac{u}{K_1} - \frac{\sigma^* B^2 u}{\rho_{hnf}} \tag{12}$$

$$\frac{\partial T}{\partial t} + u\frac{\partial T}{\partial x} + v\frac{\partial T}{\partial y} = \frac{k_{hnf}}{\left(\rho c_p\right)_{hnf}}\frac{\partial^2 T}{\partial y^2} + \frac{\mu_{hnf}}{\left(\rho c_p\right)_{hnf}}\left(\frac{\partial u}{\partial y}\right)^2 \tag{13}$$

Equation (5) with new dimensionless variables for the unsteady problem can be written as

$$\begin{cases} v = -\sqrt{\frac{c\vartheta(m+1)}{2}}x^{(m-1)/2}\left[f(\eta) + \frac{m-1}{m+1}\eta f'(\eta)\right] \\ u = cx^m f'(\eta), \eta = y\sqrt{\frac{c(m+1)}{2\vartheta}}x^{(m-1)/2} \\ \theta(\eta) = \left(T - T_\infty\right)/\left(T_w - T_\infty\right), \tau = cx^{m-1}t \end{cases} \tag{14}$$

By putting Eq. (14) into Eqs. (12–13), we have:

$$\begin{aligned}&f''' + \xi_1\left\{f''f - \frac{2m}{(m+1)}\left(f'\right)^2\right\}\\ &- \frac{2}{(m+1)}\left\{M\left(1-\phi_{Cu}\right)^{2.5}\left(1-\phi_{Fe_3O_4}\right)^{2.5} + K\right\}f'\\ &- \frac{2\xi_1}{m+1}\left[1 + (m-1)\tau\frac{\partial f}{\partial \eta}\right]\frac{\partial^2 f}{\partial\eta\partial\tau} = 0\end{aligned} \tag{15}$$

$$\begin{aligned}&\frac{\xi_2}{Pr}\theta'' + \theta' f - \frac{4m}{(m+1)}\theta f' + \xi_3 Ec\left(f''\right)^2\\ &- \frac{2}{m+1}\left[1 + (m-1)\tau\frac{\partial f}{\partial\eta}\right]\frac{\partial\theta}{\partial\tau} = 0\end{aligned} \tag{16}$$

The new corresponding boundary conditions are

$$\begin{cases} f(0,\tau) = -b\sqrt{\frac{2}{m+1}}, \frac{\partial f(0,\tau)}{\partial\eta} = \lambda, \theta(0,\tau) = 1 \\ \frac{\partial f(\eta,\tau)}{\partial\eta} \to 0, \theta(\eta,\tau) \to 0 \text{ as } \eta \to \infty \end{cases} \tag{17}$$

The unknown functions are needed to define; these functions depend on the time parameter, in order to obtain the stability of solutions

$$\begin{cases} f(\eta,\tau) = f_0(\eta) + e^{-\gamma\tau}F(\eta,\tau) \\ \theta(\eta,\tau) = \theta_0(\eta) + e^{-\gamma\tau}G(\eta,\tau) \end{cases} \tag{18}$$

where $f_0(\eta)$ and $\theta_0(\eta)$ are the small relatives of $F(\eta,\tau)$ and $G(\eta,\tau)$, respectively, which indicate the steady solutions of Eqs. (6–7). Further, γ is the unknown eigenvalue parameter, which will provide the infinite number of the values of eigenvalue. By introducing Eq. (18) into Eqs. (15–16), we get

$$\begin{aligned}&\frac{\partial^3 F}{\partial\eta^3} + \xi_1\left\{f_0\frac{\partial^2 F}{\partial\eta^2} + F\frac{d^2 f_0}{d\eta^2} - \frac{4m}{(m+1)}\frac{df_0}{d\eta}\frac{\partial F}{\partial\eta}\right\}\\ &- \frac{2}{(m+1)}\left\{M\left(1-\phi_{Cu}\right)^{2.5}\left(1-\phi_{Fe_3O_4}\right)^{2.5} + K\right\}\frac{\partial F}{\partial\eta}\\ &+ \frac{2\xi_1}{m+1}\left[1 + (m-1)\tau\frac{df_0}{d\eta}\right]\gamma\frac{\partial F}{\partial\eta} = 0\end{aligned} \tag{19}$$

$$\begin{aligned}&\frac{\xi_2}{Pr}\frac{\partial^2 G}{\partial\eta^2} + \frac{d\theta_0}{d\eta}F + \frac{\partial G}{\partial\eta}f_0 - \frac{4m}{(m+1)}\left(\theta_0\frac{\partial F}{\partial\eta} + G\frac{df_0}{d\eta}\right)\\ &+ 2Ec\xi_3\frac{d^2 f_0}{d\eta^2}\frac{\partial^2 F}{\partial\eta^2} + \frac{2}{m+1}\left[1 + (m-1)\tau\frac{df_0}{d\eta}\right]\gamma G = 0\end{aligned} \tag{20}$$

The steady solutions of the equation can be obtained by keeping $\tau = 0$, where $F(\eta,\tau)$ and $G(\eta,\tau)$ are reduced to F_0

and G_0, respectively, in Eqs. (19–20). In order to find the initial decay or growth of the solutions, we have to solve the following system of linearized eigenvalue problems

$$\xi_1 F_0''' + \xi_1\{f_0 F_0'' + F_0 f_0''\} - \frac{2}{(m+1)}\left\{M(1-\phi_{Cu})^{2.5}(1-\phi_{Fe_3O_4})^{2.5} + K\right\}F_0' + \frac{2\xi_1}{m+1}(\gamma - 2mf_0')F_0' = 0 \quad (21)$$

$$\frac{\xi_2}{Pr}G_0'' + \theta_0' F_0 + G_0' f_0 + 2Ec\xi_3 f_0'' F_0'' - \frac{4m}{(m+1)}\theta_0 F_0' + \frac{2}{m+1}(\gamma - 2mf_0')G_0 = 0 \quad (22)$$

Subject to boundary conditions

$$\begin{cases} F_0(0) = 0, F_0'(0) = 0, G_0(0) = 0 \\ F_0'(\eta) \to 0, G_0(\eta) \to 0 \text{ as } \eta \to \infty \end{cases} \quad (23)$$

Table 3 The compression of $\sqrt{Re}C_f$ with Devi and Devi [63] and Lund et al. [53]

m	ϕ_{Cu}	Devi and Devi [63]	Lund et al. [53]	Present results
1	0.005	− 1.327310	− 1.325862	− 1.3258
	0.02	− 1.409683	− 1.404648	− 1.4046
	0.04	− 1.520894	− 1.511257	− 1.5112
	0.06	− 1.634279	− 1.620177	− 1.6201
1.5	0.02	–	− 1.491175	− 1.4911
	0.04	–	− 1.604352	− 1.6043
2.5	0.02	–	− 1.585037	− 1.5850
	0.04	–	1.705327	1.7053

We followed the procedure of the Mustafa et al. [60] and Lund et al. [61], in which they stated that the one boundary condition should be relaxed to find the values of eigenvalue. In this problem, $F_0'(\eta) \to 0$ as $\eta \to \infty$ is converted into $F_0''(0) = 1$.

Results and discussion

The prime concern of the current segment is to demystify the physical importance of numerical results presented in graphical representation. Flow along with heat transfer and viscous dissipation of H_2O-based hybrid nanofluid ($Cu - Fe_3O_4$) over a nonlinear shrinking sheet has been inspected numerically with Runge–Kutta fourth order along with the shooting technique. In this study, the thermophysical properties of Devi and Devi [45] have been used as it has been proven that their results have good agreement with the experimental results of Suresh et al. [62]. Henceforth, we expect that these results would provide good direction and understanding in order to enhance the rate of heat transfer numerically and experimentally. We compared the results of coefficient of skin friction for $Al_2O_3 - Cu/H_2O$ hybrid nanofluid for different values of ϕ_{Cu} when $\phi_{Al_2O_3} = 0.1, S = 0, Pr = 6.135, \lambda = 1, M = \beta = 0$ with Devi and Devi [63] and Lund et al. [53] in order to validate the results of the current study (refer to Table 3) and found in excellent agreement. The effects of the suction parameter along with solid volume fraction of Cu and Fe_3O_4 are presented in Figs. 2–5. In Fig. 2, it can be noticed that multiple solutions exist only for the case of suction by the various intensities of copper-type nanoparticle. In this regard, the critical values of suction parameter b for $\phi_{Cu} = 0.005, 0.05, 0.1$, are $b_{c1} = -3.2064, b_{c2} = -3.0788$, and $b_{c3} = -3.0019$, respectively. Moreover, the skin friction coefficient is increased (decreased) by incorporating the copper-type nanoparticles in the base fluid for the first (second) solution. Physically, we can interpret that the velocity of nanofluid near the surface declines

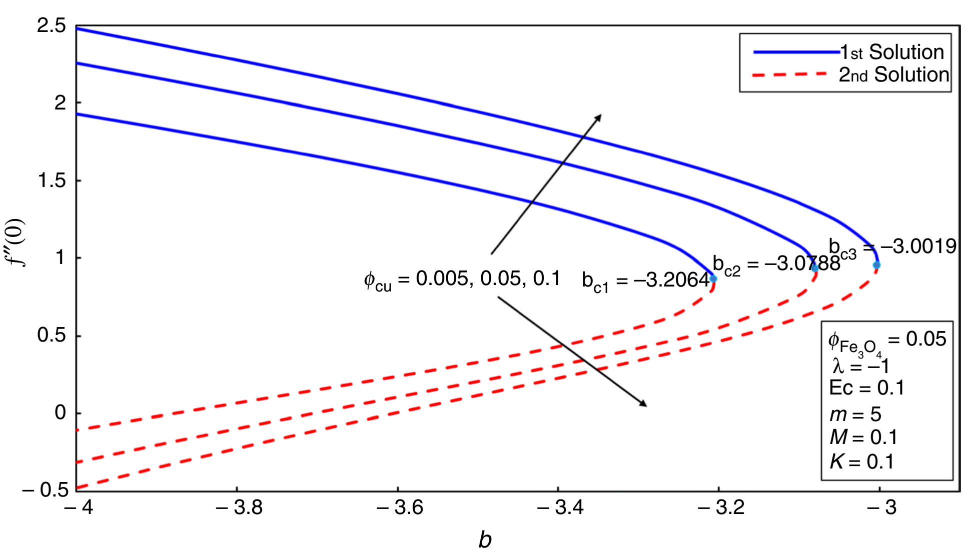

Fig. 2 Skin frictions plot with b for different ϕ_{Cu}

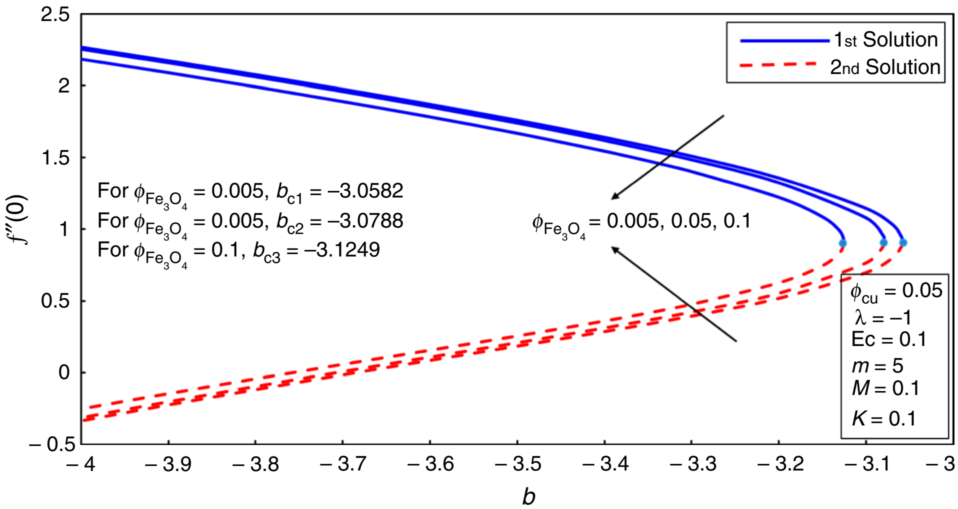

Fig. 3 Skin frictions plot with b for different $\phi_{Fe_3O_4}$

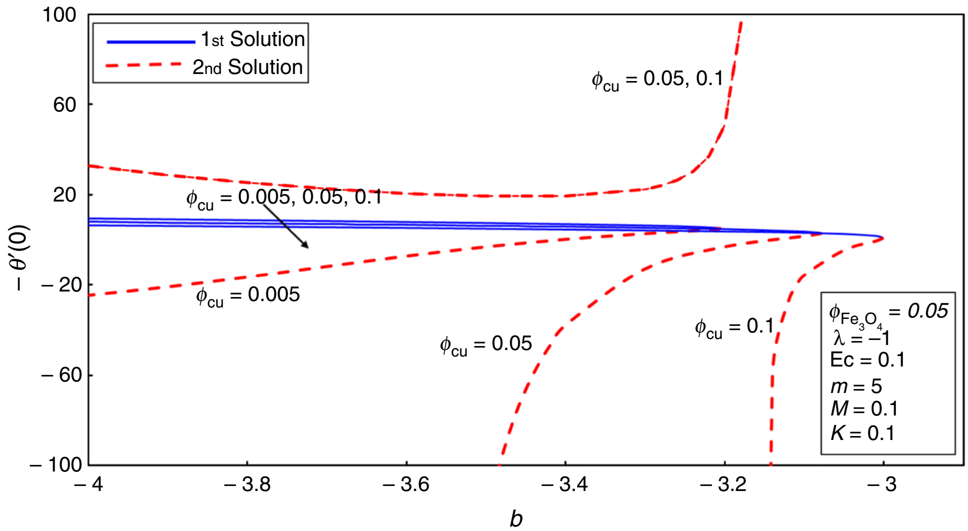

Fig. 4 Heat transfer rate plot with b for different ϕ_{Cu}

as the solid volume fraction rises in the base fluid from 0.5% to 1% only for the case of the first solution.

In the same manner, the combined effect of the suction parameter and solid volume fraction of Fe_3O_4 is plotted in Fig. 3. From this profile, it observed that the skin friction coefficient decreases (increases) by the rise in the solid volume fraction of Fe_3O_4 in the base fluid for the first (second) solution. Therefore, we can conclude that the effect of Fe_3O_4 nanoparticles on the skin friction coefficient is totally opposite to the effect of copper type nanoparticles. Hence, the velocity near the solid surface increases (decreases) in the first (second) solution. Moreover, it is also observed from this profile that dual solutions exist only for the case of suction and critical values of suction parameter b for $\phi_{Fe_3O_4} = 0.05, 0.5, 0.1$ are $b_{c1} = -3.0582, b_{c2} = -3.0788,$ and $b_{c3} = -3.1249$. Figure 4 shows the effect of heat transfer coefficient $-\theta'(0)$ with variation of b by variation of ϕ_{Cu}. It is noticed that there are regions of two solutions $b \le b_c$, and no solution range is $b > b_c$. Here, b_c is the critical value of b (10% volume fraction) where the dual solution exists. Moreover, it is noticed from this profile that the heat transfer coefficient decreases by simultaneously enhancing ϕ_{Cu} and b. It is worth to notice that due to the instability of the second solution, singularities exist as shown in the upper half of the graphs. The same scenario can be depicted in Fig. 5 for $\phi_{Fe_3O_4}$.

Figure 6 presents the effects of various values of ϕ_{Cu}- and $\phi_{Fe_3O_4}$-type nanofluids. The effects of magnetic parameter M on velocity profile $f'(\eta)$ are shown in Fig. 7. Clearly, it is seen that the velocity of the hybrid nanofluid increases as the intensity of the magnetic parameter rises gradually for the first solution and decreases for the second solution.

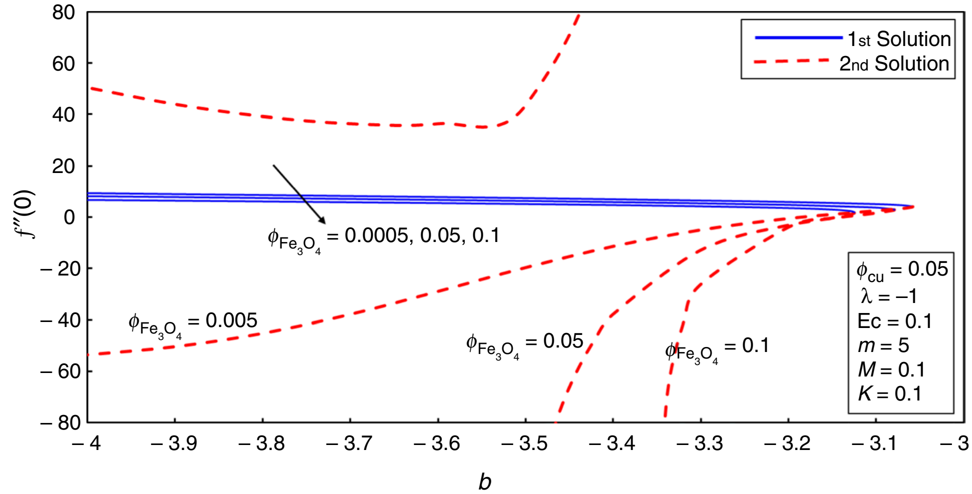

Fig. 5 Heat transfer rate plot with b for different $\phi_{Fe_3O_4}$

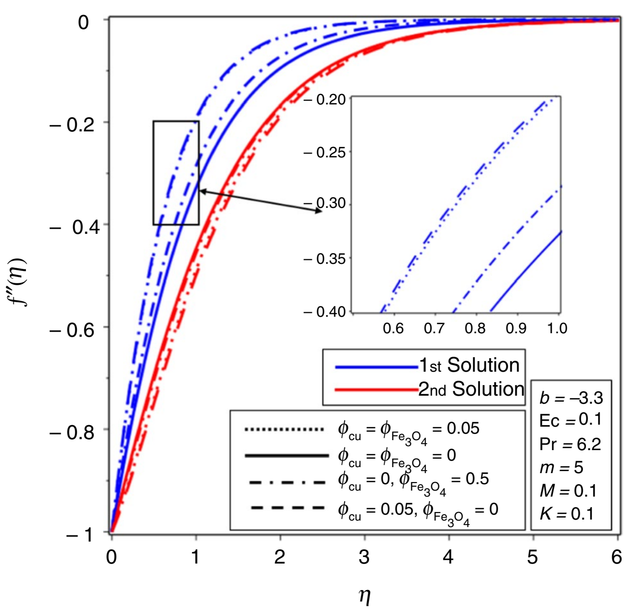

Fig. 6 Velocity plot for different values of nanoparticle volume fractions

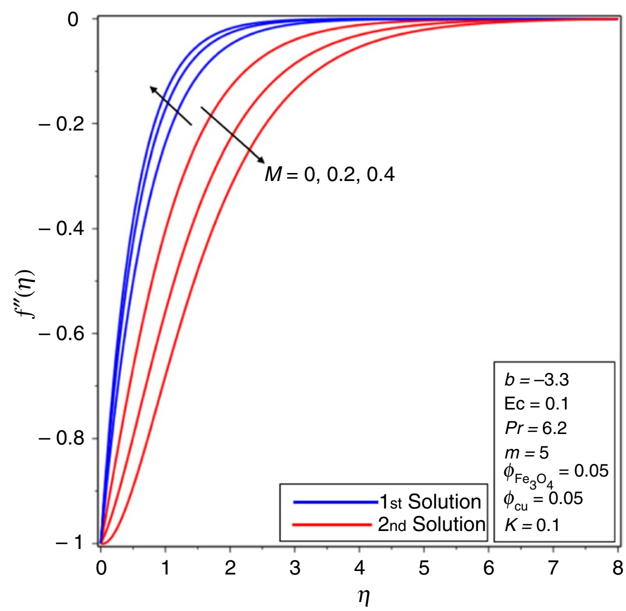

Fig. 7 Velocity plot for increasing values of M

Generally, we can say that boundary layer thickness inclines monotonically for the first solution and decreases for the second solution due to the Lorentz force which creates the resistivity on the fluid flow inside the boundary layer. Hence, the motion of solid nanoparticles diminishes. Figure 8 presents the effects of permeability coefficient on velocity profile. It is seen that at higher values of permeability the velocity of hybrid nanofluid deaccelerates in the first solution and accelerates for the second solution. The impact of power index m can be seen in Fig. 9 on velocity profile. It is perceived that as power index $m \geq 1$, the boundary layer thickness rises gradually and therefore velocity of the hybrid nanoparticles increases for both solutions.

Figure 10 elucidates the effect of ϕ_{Cu} and $\phi_{Fe_3O_4}$ on temperature profile $\theta(\eta)$. It is realized from this graph that for the case of simple viscous fluid where the intensity of ϕ_{Cu} and $\phi_{Fe_3O_4}$ are negligible (i.e., $\phi_{Cu} = \phi_{Fe_3O_4} = 0$), the temperature profile is much lower. In other words, the thermal boundary layer thickness of viscous fluid is lower as compared to hybrid nanofluid. Moreover, it is worthy to notify that the thermal boundary layer becomes thicker for a 5% suspension of nanoparticles of Cu and Fe_3O_4 in the base fluid. Similarly, the upshot of the magnetic parameter M on temperature profile is depicted in Fig. 11. In the first solution, the temperature of the hybrid nanofluid increases as the strength of the magnetic parameter M increases. From the physical aspect, we can say that the rise in the magnetic parameter

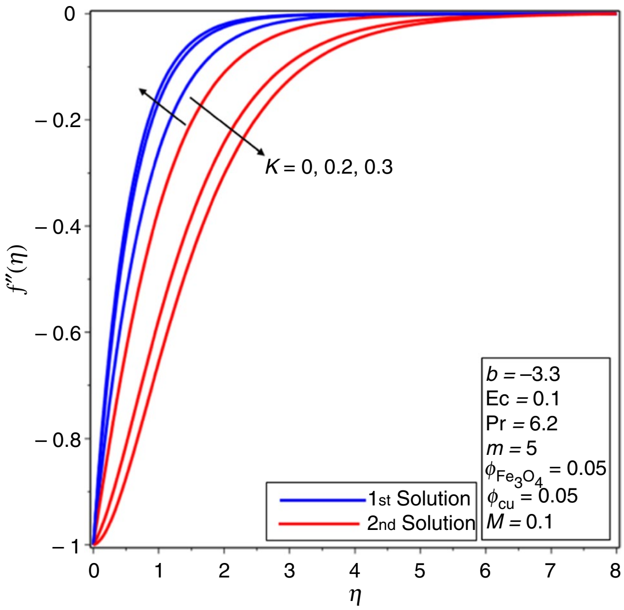

Fig. 8 Velocity plot for increasing values of K

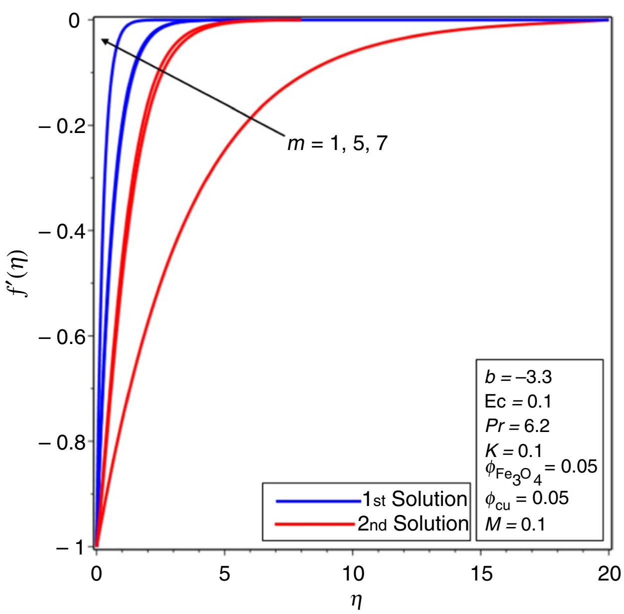

Fig. 9 Velocity plot for increasing values of m

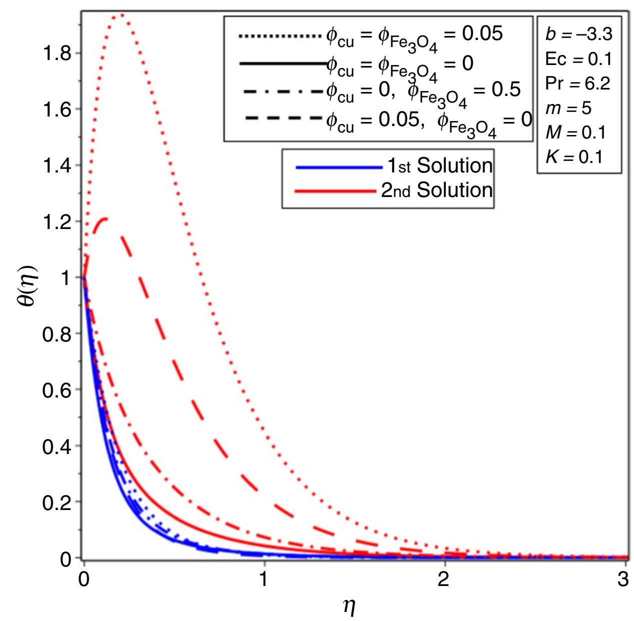

Fig. 10 Temperature plot for different values of nanoparticle volume fractions

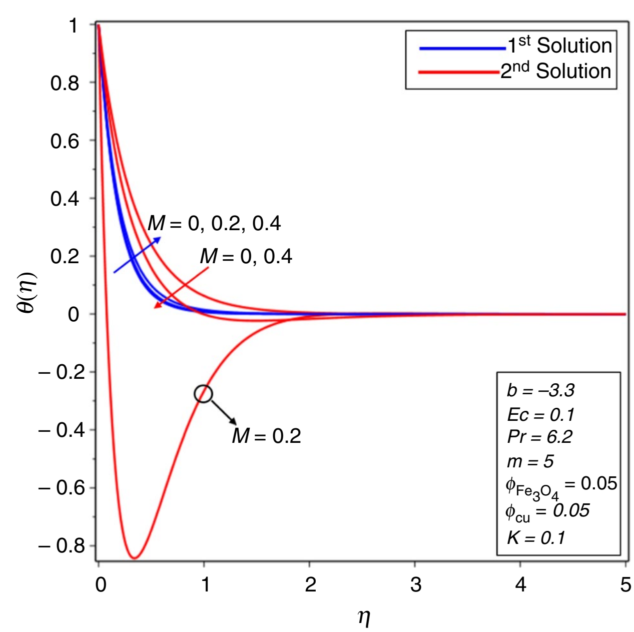

Fig. 11 Temperature plot for increasing values of M

produces the Lorentz force which contributes to increase in the temperature of the fluid due to the slowdown of the fluid motion. Similar behavior of temperature profile can be seen in Fig. 12 for the variation of permeability parameter K. Outcomes of power index m and Eckert number Ec on temperature profile are plotted in Figs. 13 and 14, respectively. From these graphs, it is noticed that the temperature profile of hybrid nanofluid is directly proportional to power index m and Eckert number Ec. Physically, the thickness of the thermal layer, as well as the temperature of the fluid increase due to the high intensity of kinetic energy as Eckert number, is directly proportional to the kinetic energy.

Finally, Table 4 gives the values of the smallest eigenvalue for variation of suction parameter. It can be concluded easily that the first solution is the stable one as the sign of the value

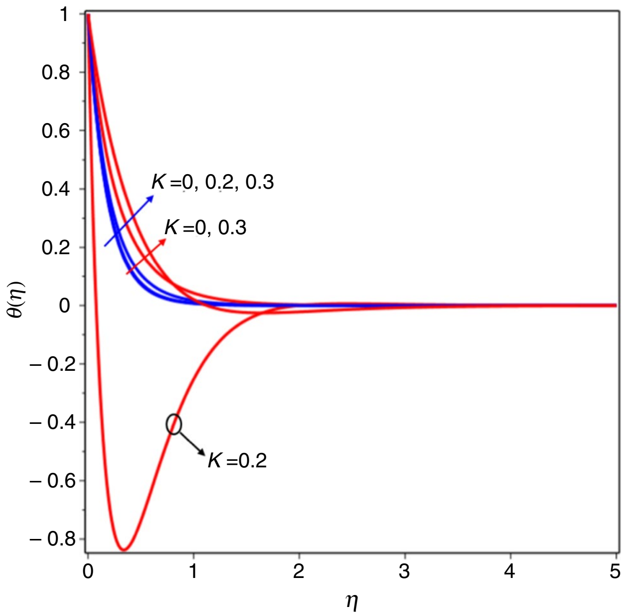

Fig. 12 Temperature plot for increasing values of K

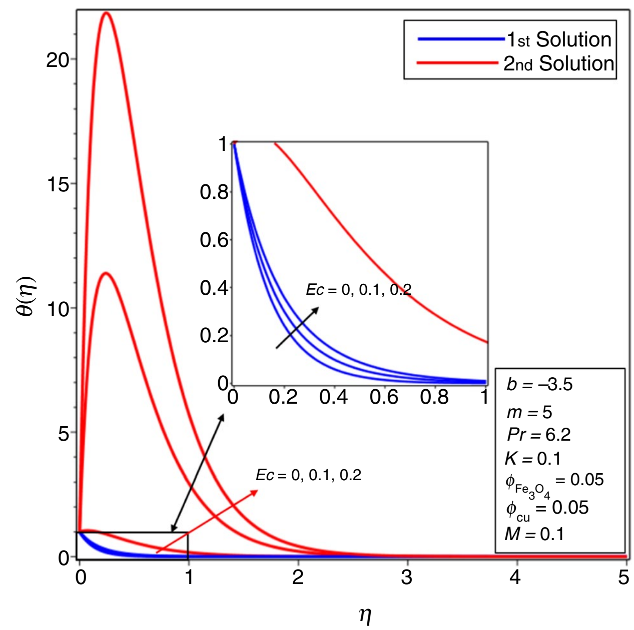

Fig. 14 Temperature plot for increasing values of Ec

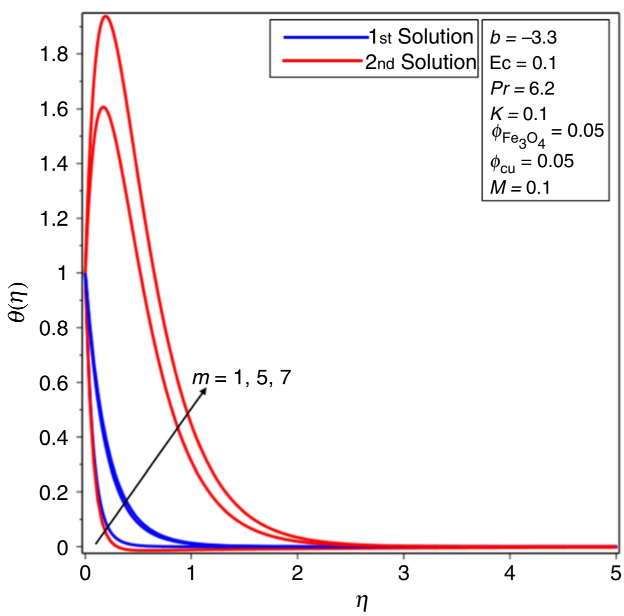

Fig. 13 Temperature plot for increasing values of m

of the smallest eigenvalue is positive which shows the initial decay, while in the second solution, the sign of the values of the smallest eigenvalue is negative, indicating the existence of the initial growth of disturbance which causes the solution to be unstable.

Table 4 The smallest eigenvalues γ for the several values of suction parameter b at $\phi_{Cu} = \phi_{Al_2O_3} = 0.05$ $m = 5, \mathrm{Pr} = 6.2, \mathrm{Ec} = M = K = 0.1$ and $\lambda = -1$

b	γ	
	First solution	Second solution
−4	1.6135	−1.2369
−3.8	1.3074	−1.0891
−3.6	1.0087	−0.8257
−3.4	0.8523	−0.6393
−3.2	0.4237	−0.5286
−3	0.0530	−0.0904
−3.0788	0.0009	−0.0023

Conclusions

In the current study, 2D steady MHD flow of $Cu-Fe_3O_4/H_2O$ hybrid nanofluid over the nonlinear stretching/shrinking surface has been examined. The effects of energy dissipation function and porous term also have been taken into account. Similarity variables are used to change the partial differential equations (PDEs) into ODEs. ODEs are solved by employing the shooting method with the RK fourth-order method. For the stability of solutions, a three-stage Lobatto IIIa formula has been used to find the values of the smallest eigenvalue. In light of the present examination, the following points are the major findings of this study.

1. There is a region of dual solutions that depend upon the suction and stretching/shrinking parameters, respectively.
2. The results of the stability analysis reveal that the first solution is more stable as compared to the second solution.
3. The rate of heat transfer reduces when suction and solid volume fraction of copper are increased.
4. The thickness of the hydrodynamic boundary layer increases for the intensive impact of the magnetic field, permeability, and power index parameter in the first solution, while reverse nature of velocity profiles is noticed in the second solution when the magnetic field and permeability parameters have risen.
5. The temperature of hybrid nanofluid is high in the first solution when the magnetic field, power index parameter, and Eckert number increase.

Acknowledgements This research is supported by Universiti Utara Malaysia. The first author is thankful to the School of Quantitative Sciences (SQS) for providing easy access to the postgraduate lab to conduct and complete this research, special thanks to Prof. Zurni Omar and Prof. Ilyas Khan.

References

1. Mabood F, Khan WA, Ismail AM. MHD boundary layer flow and heat transfer of nanofluids over a nonlinear stretching sheet: a numerical study. J Magn Magn Mater. 2015;374:569–76.
2. Devi NP, Rao CS, Kumar KK. Numerical and experimental studies of nanofluid as a coolant flowing through a circular tube. In: Numerical heat transfer and fluid flow. Singapore: Springer; 2019. p. 511–518.
3. Khan U, Zaib A, Khan I, Nisar KS. Activation energy on MHD flow of titanium alloy (Ti6Al4V) nanoparticle along with a cross flow and streamwise direction with binary chemical reaction and non-linear radiation: dual solutions. J Mater Res Technol. 2020;9(1):188–99.
4. Khan A, Ali HM, Nazir R, Ali R, Munir A, Ahmad B, Ahmad Z. Experimental investigation of enhanced heat transfer of a car radiator using ZnO nanoparticles in H_2O–ethylene glycol mixture. J Therm Anal Calorim. 2019;138(5):3007–211.
5. Meva FE, Ntoumba AA, Kedi PB, Tchoumbi E, Schmitz A, Schmolke L, Klopotowski M, Moll B, Kökcam-Demir Ü, Mpondo EA, Lehman LG. Silver and palladium nanoparticles produced using a plant extract as reducing agent, stabilized with an ionic liquid: sizing by X-ray powder diffraction and dynamic light scattering. J Mater Res Technol. 2019;8(2):1991–2000.
6. Shah TR, Ali HM. Applications of hybrid nanofluids in solar energy, practical limitations and challenges: a critical review. Sol Energy. 2019;183:173–203.
7. Ruhani B, Toghraie D, Hekmatifar M, Hadian M. Statistical investigation for developing a new model for rheological behavior of ZnO–Ag (50%–50%)/Water hybrid Newtonian nanofluid using experimental data. Physica A. 2019;525:741–51.
8. Mahian O, Kolsi L, Amani M, Estellé P, Ahmadi G, Kleinstreuer C, Marshall JS, Siavashi M, Taylor RA, Niazmand H, Wongwises S. Recent advances in modeling and simulation of nanofluid flows-part I: fundamentals and theory. Phys Rep. 2019;790:1–48.
9. Ranjbarzadeh R, Moradikazerouni A, Bakhtiari R, Asadi A, Afrand M. An experimental study on stability and thermal conductivity of water/silica nanofluid: eco-friendly production of nanoparticles. J Clean Prod. 2019;206:1089–100.
10. Lund LA, Omar Z, Khan I, Sherif ES. Dual solutions and stability analysis of a hybrid nanofluid over a stretching/shrinking sheet executing MHD flow. Symmetry. 2020;12(2):276.
11. Alarifi IM, Nguyen HM, Naderi Bakhtiyari A, Asadi A. Feasibility of ANFIS-PSO and ANFIS-GA models in predicting thermophysical properties of Al_2O_3–MWCNT/Oil hybrid nanofluid. Materials. 2019;12(21):3628.
12. Rosmila AB, Kandasamy R, Muhaimin I. Lie symmetry group transformation for MHD natural convection flow of nanofluid over linearly porous stretching sheet in presence of thermal stratification. Appl Math Mech. 2012;33(5):593–604.
13. Sivakumar N, Prasad PD, Raju CS, Varma SV, Shehzad SA. Partial slip and dissipation on MHD radiative ferro-fluid over a nonlinear permeable convectively heated stretching sheet. Results Phys. 2017;7:1940–9.
14. Abdelrazek AH, Kazi SN, Alawi OA, Yusoff N, Oon CS, Ali HM. Heat transfer and pressure drop investigation through pipe with different shapes using different types of nanofluids. J Therm Anal Calorim. 2020;139(3):1637–53.
15. Ali HM. Thermal performance analysis of metallic foam-based heat sinks embedded with RT-54HC paraffin: an experimental investigation for electronic cooling. J Therm Anal Calorim. 2019;4:1–2.
16. Ghanbari B, Kumar S, Kumar R. A study of behaviour for immune and tumor cells in immunogenetic tumour model with non-singular fractional derivative. Chaos Solitons Fractals. 2020;133:109619.
17. Lund LA, Omar Z, Khan I, Dero S. Multiple solutions of Cu–$C_6H_9NaO_7$ and Ag–$C_6H_9NaO_7$ nanofluids flow over nonlinear shrinking surface. J Central South Univ. 2019;26(5):1283–93.
18. Bhatta DP, Mishra SR, Dash JK. Unsteady squeezing flow of water-based nanofluid between two parallel disks with slip effects: Analytical approach. Heat Transf Asian Res. 2019;48(5):1575–94.
19. Hayat T, Hussain Z, Alsaedi A, Asghar S. Carbon nanotubes effects in the stagnation point flow towards a nonlinear stretching sheet with variable thickness. Adv Powder Technol. 2016;27(4):1677–88.
20. Selimefendigil F, Oztop HF, Sheremet MA, Abu-Hamdeh N. Forced convection of Fe_3O_4–water nanofluid in a bifurcating channel under the effect of variable magnetic field. Energies. 2019;12(4):666.
21. Kristiawan B, Wijayanta AT, Enoki K, Miyazaki T, Aziz M. Heat transfer enhancement of TiO_2/water nanofluids flowing inside a square minichannel with a microfin structure: a numerical investigation. Energies. 2019;12(16):3041.
22. Dero S, Rohni AM, Saaban A. The dual solutions and stability analysis of nanofluid flow using tiwari-das modelover a permeable exponentially shrinking surface with partial slip conditions. J Eng Appl Sci. 2019;14:4569–82.
23. Sharma B, Kumar S, Paswan MK. Analytical solution for mixed convection and MHD flow of electrically conducting non-Newtonian nanofluid with different nanoparticles: a comparative study. Int J Heat Technol. 2018;36(3):987–96.
24. De P. Impact of dual solutions on nanofluid containing motile gyrotactic micro-organisms with thermal radiation. BioNanoScience. 2019;9(1):13–20.
25. Sharma B, Kumar S, Cattani C, Baleanu D. Nonlinear dynamics of Cattaneo–Christov heat flux model for third-grade power-law fluid. J Comput Nonlinear Dyn. 2020;15(1):011009.
26. Hassan A, Wahab A, Qasim MA, Janjua MM, Ali MA, Ali HM, Jadoon TR, Ali E, Raza A, Javaid N. Thermal management and uniform temperature regulation of photovoltaic modules using

hybrid phase change materials-nanofluids system. Renew Energy. 2020;145:282–93.
27. Lund LA, Omar Z, Khan I. Mathematical analysis of magnetohydrodynamic (MHD) flow of micropolar nanofluid under buoyancy effects past a vertical shrinking surface: dual solutions. Heliyon. 2019;5(9):e02432.
28. Dero S, Uddin MJ, Rohni AM. Stefan blowing and slip effects on unsteady nanofluid transport past a shrinking sheet: multiple solutions. Heat Transf Asian Res. 2019;48(6):2047–66.
29. Sajid MU, Ali HM, Sufyan A, Rashid D, Zahid SU, Rehman WU. Experimental investigation of TiO_2–water nanofluid flow and heat transfer inside wavy mini-channel heat sinks. J Therm Anal Calorim. 2019;137(4):1279–94.
30. Buongiorno J. Convective transport in nanofluids. J Heat Transf. 2006;128(3):240–50.
31. Tiwari RK, Das MK. Heat transfer augmentation in a two-sided lid-driven differentially heated square cavity utilizing nanofluids. Int J Heat Mass Transf. 2007;50(9–10):2002–188.
32. Khashi'ie NS, Md Arifin N, Nazar R, Hafidzuddin EH, Wahi N, Pop I. A stability analysis for magnetohydrodynamics stagnation point flow with zero nanoparticles flux condition and anisotropic slip. Energies. 2019;12(7):1268.
33. Jamaludin A, Nazar R, Pop I. Mixed convection stagnation-point flow of a nanofluid past a permeable stretching/shrinking sheet in the presence of thermal radiation and heat source/sink. Energies. 2019;12(5):788.
34. Ali Lund L, Ching DL, Omar Z, Khan I, Nisar KS. Triple local similarity solutions of Darcy-Forchheimer Magnetohydrodynamic (MHD) flow of micropolar nanofluid over an exponential shrinking surface: stability analysis. Coatings. 2019;9(8):527.
35. Raza J, Rohni AM, Omar Z, Awais M. Heat and mass transfer analysis of MHD nanofluid flow in a rotating channel with slip effects. J Mol Liq. 2016;219:703–8.
36. Salleh SN, Bachok N, Arifin NM, Ali FM, Pop I. Magnetohydrodynamics flow past a moving vertical thin needle in a nanofluid with stability analysis. Energies. 2018;11(12):3297.
37. Kumar S, Kumar A, Abbas S, Al Qurashi M, Baleanu D. A modified analytical approach with existence and uniqueness for fractional Cauchy reaction–diffusion equations. Adv Differ Equ. 2020;220(1):1–8.
38. Lund LA, Omar Z, Khan I. Quadruple solutions of mixed convection flow of magnetohydrodynamic nanofluid over exponentially vertical shrinking and stretching surfaces: Stability analysis. Comput Methods Programs Biomed. 2019;182:105044.
39. Rasool G, Zhang T. Characteristics of chemical reaction and convective boundary conditions in Powell–Eyring nanofluid flow along a radiative Riga plate. Heliyon. 2019;5(4):e01479.
40. Raza J, Rohni AM, Omar Z. Rheology of micropolar fluid in a channel with changing walls: Investigation of multiple solutions. J Mol Liq. 2016;223:890–902.
41. Jamaludin A, Nazar R, Pop I. Three-dimensional magnetohydrodynamic mixed convection flow of nanofluids over a nonlinearly permeable stretching/shrinking sheet with velocity and thermal slip. Appl Sci. 2018;8(7):1128.
42. Tlili I, Bhatti MM, Hamad SM, Barzinjy AA, Sheikholeslami M, Shafee A. Macroscopic modeling for convection of Hybrid nanofluid with magnetic effects. Physica A. 2019;534:122136.
43. Ahmadi MH, Ghazvini M, Sadeghzadeh M, Nazari MA, Ghalandari M. Utilization of hybrid nanofluids in solar energy applications: a review. Nano Struct Nano Objects. 2019;20:100386.
44. Ahmed N, Saba F, Khan U, Khan I, Alkanhal TA, Faisal I, Mohyud-Din ST. Spherical shaped ($Ag-Fe_3O_4/H_2O$) hybrid nanofluid flow squeezed between two Riga plates with nonlinear thermal radiation and chemical reaction effects. Energies. 2019;12(1):76.
45. Devi SA, Devi SS. Numerical investigation of hydromagnetic hybrid $Cu–Al_2O_3$/water nanofluid flow over a permeable stretching sheet with suction. Int J Nonlinear Sci Numer Simul. 2016;17(5):249–57.
46. Waini I, Ishak A, Pop I. Hybrid nanofluid flow and heat transfer over a nonlinear permeable stretching/shrinking surface. Int J Numer Methods Heat Fluid Flow. 2019;59(1):91–9.
47. Waini I, Ishak A, Pop I. Unsteady flow and heat transfer past a stretching/shrinking sheet in a hybrid nanofluid. Int J Heat Mass Transf. 2019;136:288–97.
48. Bhattacharyya K, Vajravelu K. Stagnation-point flow and heat transfer over an exponentially shrinking sheet. Commun Nonlinear Sci Numer Simul. 2012;17(7):2728–34.
49. Khashi'ie NS, Arifin NM, Nazar R, Hafidzuddin EH, Wahi N, Pop I. Magnetohydrodynamics (MHD) axisymmetric flow and heat transfer of a hybrid nanofluid past a radially permeable stretching/shrinking sheet with joule heating. Chin J Phys. 2019;64:251–63.
50. Yahaya RI, Arifin NM, Nazar R, Pop I. Flow and heat transfer past a permeable stretching/shrinking sheet in $Cu-Al_2O_3$/water hybrid nanofluid. Int J Numer Meth Heat Fluid Flow. 2019;30(3):1197–222.
51. Aly EH, Pop I. MHD flow and heat transfer over a permeable stretching/shrinking sheet in a hybrid nanofluid with a convective boundary condition. Int J Numer Meth Heat Fluid Flow. 2019;29(9):3012–38.
52. Hayat T, Nadeem S, Khan AU. Aspects of 3D rotating hybrid CNT flow for a convective exponentially stretched surface. Appl Nanosci. 2019. https://doi.org/10.1007/s13204-019-01036-y.
53. Lund LA, Omar Z, Khan I, Seikh AH, Sherif ES, Nisar KS. Stability analysis and multiple solution of $Cu–Al_2O_3/H_2O$ nanofluid contains hybrid nanomaterials over a shrinking surface in the presence of viscous dissipation. J Mater Res Technol. 2020;9(1):421–32.
54. Rana P, Shukla N, Gupta Y, Pop I. Homotopy analysis method for predicting multiple solutions in the channel flow with stability analysis. Commun Nonlinear Sci Numer Simul. 2019;66:183–93.
55. Lund LA, Omar Z, Khan I. Analysis of dual solution for MHD flow of Williamson fluid with slippage. Heliyon. 2019;5(3):e01345.
56. Khan AU, Hussain ST, Nadeem S. Existence and stability of heat and fluid flow in the presence of nanoparticles along a curved surface by mean of dual nature solution. Appl Math Comput. 2019;353:66–81.
57. Abu Bakar NA, Bachok N, Md Arifin AN. Boundary layer stagnation-point flow over a stretching/shrinking cylinder in a nanofluid: a stability analysis. Indian J Pure Appl Phys (IJPAP). 2019;57(2):106–17.
58. Mustafa I, Javed T, Ghaffari A, Khalil H. Enhancement in heat and mass transfer over a permeable sheet with Newtonian heating effects on nanofluid: multiple solutions using spectral method and stability analysis. Pramana. 2019;93(4):53.
59. Lund LA, Omar Z, Dero S, Khan I. Linear stability analysis of MHD flow of micropolar fluid with thermal radiation and convective boundary condition: exact solution. Heat Transf Asian Res. 2020;49(1):461–76.
60. Mustafa I, Abbas Z, Arif A, Javed T, Ghaffari A. Stability analysis for multiple solutions of boundary layer flow towards a shrinking sheet: analytical solution by using least square method. Physica A. 2020;540:123028.
61. Lund LA, Omar Z, Khan I. Steady incompressible magnetohydrodynamics Casson boundary layer flow past a permeable vertical and exponentially shrinking sheet: a stability analysis. Heat Transf Asian Res. 2019;48(8):3538–56.
62. Suresh S, Venkitaraj KP, Selvakumar P, Chandrasekar M. Synthesis of Al_2O_3–Cu/water hybrid nanofluids using two step method and its thermo physical properties. Coll Surf A Physicochem Eng Asp. 2011;388(1–3):41–8.

63. Devi SU, Devi SA. Heat transfer enhancement of $Cu-Al_2O_3$/water hybrid nanofluid flow over a stretching sheet. J Niger Math Soc. 2017;36(2):419–33.